XLI CILAMCE
XLI Ibero-Latin American Congress on Computational Methods in Engineering
16-19 November, 2020 FOZ DO IGUAÇU PARANÁ - BRAZIL

# Finite element models for analysis of structural integrity of onshore wind turbine foundations with embedded rings submitted to static and dynamic loads.

Thaís Tenório Dourado[1], Windson Bezerra de Aguiar[1], Paulo Marcelo Vieira Ribeiro[1]

[1]*Department of Civil Engineering, Federal University of Pernambuco - UFPE*
*Avenida da Arquitetura s/n, 50740-550, Pernambuco/Recife, Brasil*
*thais.tdourado@gmail.com, windson.aguiar@yahoo.com.br, paulo.vribeiro@ufpe.br*

**Abstract.** Wind turbines' share in the energy industry continues to grow, its status of renewable energy source deeming it attractive due to environmental policies established worldwide. Most of these turbines are onshore installations and are supported by steel towers connected to reinforced concrete foundations through embedded rings (or insert rings), a type of structure with reported damages to the tower-foundation interface. This study presents simulation procedures for this kind of foundation concerning their structural behavior. Emphasis is given on the development of finite element models with the aid of the finite element software Abaqus. First, a linear 3D model considering only equivalent static loads transferred through the embedded ring. Then, after estimation of aerodynamic loads, a linear dynamic analysis. This methodology provides a valuable resource since the knowledge of the model's response to different load scenarios can be used to prevent deterioration in embedded ring foundations, and future advances can guide maintenance and rehabilitation plans on existing wind turbine farms.

**Keywords:** Wind turbine foundations; Finite element models; Embedded rings; Structural dynamics.

## 1 Introduction

In the current social and economic context of high demand for renewable energies, wind turbines play a significant part. From the available supporting structures, the embedded ring foundation is currently present in the bulk of wind turbine projects, according to He *et al.* [1], and was the primary choice of the industry since the beginning, as reported by Hassanzadeh [2]. Works published reporting damages in the concrete surrounding the bottom flange of the ring invokes a more profound knowledge of those structures and their behavior to avoid safety risks, interruption of electricity generation, and further high costs associated with repair.

Some researchers who studied sensor implementation to monitor a foundation structural activity highlighted the high levels of vertical displacements detected, like Currie *et al.* [3,4], and the participation of the cyclic wind loads in deteriorating the affected regions, as He *et al.* [1]. The damages detected relate to the primary function of the steel ring: to transmit turbine and tower loads into the base and, subsequently, the ground. Encouraged by this scenario, this research paper will present finite element models of the foundation analyzed under two load conditions: static and dynamic. First, it will describe the embedded ring foundation, the numerical model, and the load cases' development. Then, the simulations' procedures, along with the results and pertinent discussions.

## 2 Theoretical and computational background

### 2.1 Embedded ring foundation

The majority of the wind energy plants are made of onshore wind turbines, which can be supported by

different tower concepts, with tubular steel structures classified as the most commonly allotted type by Hassandzadeh [2]. These steel towers stand on reinforced concrete foundations: generally, spread footings directly overloading the soil, if it has bearing capacity, or transferring its loads into piles. In the case of embedded ring foundations, the connection between tower and concrete base occurs via a metallic ring structure, over whose top flange the bottom section of the tubular tower can be bolted through (Figure 1).

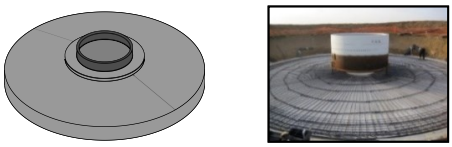

Figure 1. Embedded ring foundation

## 2.2 Numerical model and hypothesis

A numerical model aims to represent the behavior of real-life systems, and the finite element method is particularly useful as a model for solving engineering problems when an analytical solution is too complex or unavailable. It approximates the solution of differential equations to the solution of simultaneous algebraic ones for a structure discretized into small units: the finite elements (Logan [5]).

Figure 2 illustrates the translation of a real onshore wind turbine into the numerical model of the foundation analyzed in this project. All loads acting on the superstructure are transported to the foundation, considered to lie above a completely rigid soil. The model of the structure was discretized into linear hexahedral 3D elements (Figure 3). Each element has eight corner nodes with three translational degrees of freedom each. Rao [6] develops the element from the elasticity equations of equilibrium combined with the stress/strain and kinematic relationships. The mathematical formulation discussed is omitted in this paper since the research was conducted in a Finite Element Analysis (FEA) software with element technologies already established.

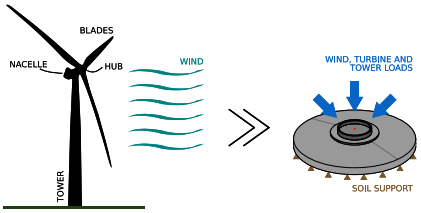


Figure 2. Real wind turbine under wind conditions (left); numerical model (right)

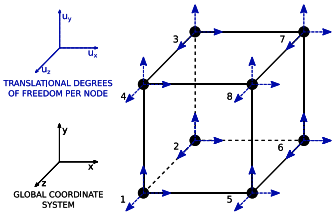


Figure 3. Linear hexahedral element

## 2.3 Case study data

The numerical model presented builds over a preliminary structural design of an embedded ring foundation, whose geometric data is a replica from the foundation slab in Svensson's [7] work. Accordingly, it is assumed to support the same wind turbine as in this referenced project: a Vestas V-90 of 2MW. Relevant turbine information extracted from the product's brochure [8] and foundation details in Table 1 and Figure 4, respectively.

Table 1. V90 - 2MW wind turbine specifications [8]

| **Operating data** | | **Rotor** | | **Tower** | |
|---|---|---|---|---|---|
| Rated power | 2000 kW | Rotor diameter | 90 m | Type | Tubular steel |
| Cut-in wind speed | 4 m/s | Swept area | 6362 m² | Hub height | 80 m |
| Rated wind speed | 12 m/s | Blade length | 44 m | Weight | 148 t |
| Cut-out wind speed | 25 m/s | Blade weight | 6700 kg | **Nacelle** | |
| | | Hub weight | 18 t | Weight | 18 t |

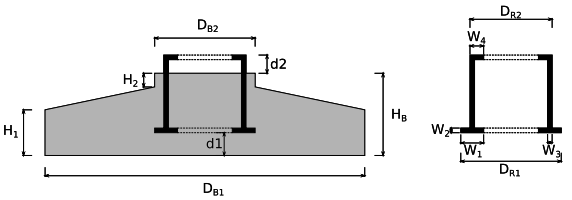


| | | | | | |
|---|---|---|---|---|---|
| $D_{B1}$ | = | 15 m | $D_{R1}$ | = | 4.48 m |
| $D_{B2}$ | = | 6 m | $D_{R2}$ | = | 2.094 m |
| **H** | = | 2.52 m | $W_1$ | = | 0.33 m |
| $H_1$ | = | 1.25 m | $W_2$ | = | 0.075 m |
| $H_2$ | = | 0.27 m | $W_3$ | = | 0.038 m |
| $d_1$ | = | 0.77 m | $W_4$ | = | 0.184 m |
| $d_2$ | = | 0.55 m | | | |

Figure 4. Detailing of the preliminary foundation design

## 2.4 Static loads

The loads acting on the foundation can be categorized into gravitational and wind loads. For the static analysis, the gravitational load arriving on the foundation top was taken as the sum of the turbine and the tower weights from the turbine's specifications [8]. Table 2 summarizes the procedure followed.

Table 2. Gravitational loads

| Elements | Mass (kg) | Comments |
|---|---|---|
| Blades | 20100 | Total of three (Each blade: 6700 kg) |
| Nacelle | 70000 | |
| Hub | 18000 | |
| Tower | 148000 | 80m tower |
| Total: | 256100 | |
| Mass: | 263783 | 248417 kg - 263783 kg: Range of total mass for 3% tolerance ([9]) |
| $F_V$ (kN): | 2586.8276 | For gravitational acceleration: g= 9.8066 m/s$^2$ |

The aerodynamic loads first had to be considered static. Figure 5 shows these wind forces and their equivalent static loads on the top of the foundation when the turbine is modeled as a fixed-free cantilever. They result from eqs. (1) and (2) which represent, respectively, the culminating horizontal force and overturning moment from the thrust (T) acting on the turbine blades and the wind profile (V(z)) acting over the tower, as derived by Kawai *et al*. [10] and Perry *et al.* [11].

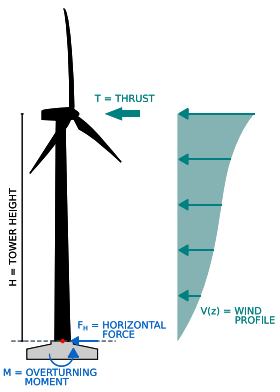


Figure 5. Schematics for the equivalent static wind loads acting on foundation top

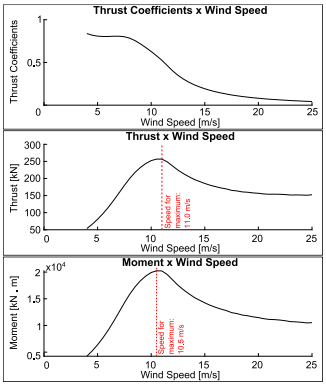


Figure 6. Thrust coefficients [9] (top), horizontal force (middle) and overturning moment (bottom) distributed over operational wind speeds

$$F_H = \frac{1}{2}\rho V_0^2 C_t A + \int_0^H \frac{1}{2}\rho V(z)^2 C_{fx} \mathrm{D}_t(z)\mathrm{d}z\,, \tag{1}$$

$$M = \frac{\rho V_0^2 C_t A H}{2} + \int_0^H \frac{\rho V(z)^2 C_{fx} \mathrm{D}_t(z) z}{2}\mathrm{d}z\,, \tag{2}$$

where:

| | | | | | | | | |
|---|---|---|---|---|---|---|---|---|
| $V_0$ | : | wind speed | H | : | hub height | $C_t$ | : | thrust coefficient |
| V(z) | : | wind speed profile | $D_t(z)$ | : | tower diameter | $C_{fx}$ | : | drag coefficient |
| A | : | swept area | ρ | : | air density | | | |

For the sake of simplicity, the wind profile for stable wind conditions ( $V(z) = V_0(\frac{z}{H})^{(\frac{1}{7})}$ ) and a constant tower diameter, $D_t(z)$, are considered, similarly to Perry *et al.* [11]. The expressions then result in eqs. (3) and (4):

$$F_H = \frac{\rho V_0^2 (7 C_{fx} D_t H + 9 A C_t)}{18}, \tag{3}$$

$$M = \frac{\rho V_0^2 H (7 C_{fx} D_t H + 16 A C_t)}{32}. \tag{4}$$

The thrust coefficients ($C_t$) vary with the operational velocity ($V_0$) according to relations provided by the manufacturer (Figure 6, top) [9]. Therefore, the overturning moment and horizontal force expressions must be evaluated for each pair of $C_t$ -$V_0$ (results in Figure 6, middle and bottom) and the maximum possible operational load can then be determined. Relevant parameters and results are in Table 3.

Table 3. Values for parameters in Eqs.(3), (4), and static equivalent wind loads

| Parameter | Value | Units | Comments |
|---|---|---|---|
| ρ | 1.225 | kg/m³ | Air density at sea level |
| $V_0$ | 10.5 | m/s | Speed for maximum overturning moment [Eq. 4; Figure 6] |
| H | 80 | m | Hub / tower height |
| $C_{fx}$ | 0.5 | - | Approximation from mean drag coefficients in KONO *et al.* [11] |
| $D_t$ | 4 | m | Largest tower diameter |
| $C_t$ | 0.578 | - | Thrust coefficient corresponding to $V_0$ |
| A | 6361.73 | m² | Area swept by the turbine blades |
| $F_H$ = | 256.7096 | kN | M = 20242.6474 kN . m |

## 2.5 Dynamic loads

For the structure's dynamic response, the loads were estimated based on the strategy presented by Barros [12]. For that reason, only the thrust is present in this analysis. The approach begins with the generation of a Kaimal turbulent wind spectrum around the wind speed responsible for the highest thrust during operation. To obtain the thrust on the rotor for each operating wind speed (and its corresponding overturning moment), the procedure is similar to the one described for the static loads. The difference lies in the absence of the wind profile effect on the tower, which results in eqs. (5) and (6) for the horizontal force and moment expressions, respectively.

With the help of a MATLAB script from Kjørlaug [13], adapted for this research, a random wind spectrum (Figure 7) is generated to combine with the thrust-velocity relations emerging from eqs. (5) and (6). The resulting aerodynamic loads can be seen in Figure 8 and Figure 9.

$$F_H = \frac{\rho V_0^2 C_t A}{2} \tag{5}$$

$$M = \frac{\rho V_0^2 C_t A H}{2} \tag{6}$$

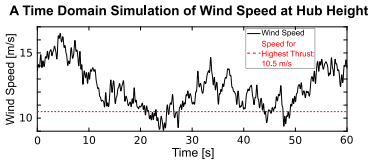


Figure 7. Wind spectrum

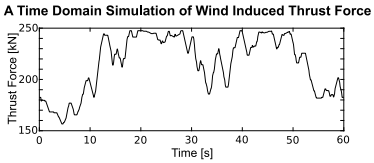


Figure 8. Horizontal force

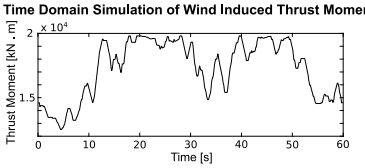


Figure 9. Overturning moment

# 3 Numerical experiments and results

This project methodology focused on the progressive validation of consecutive steps to ensure valid blocks before advancing towards the linear-static and linear-dynamic analysis. The critical points in the simulation procedures, common to both analyses, are described next.

## 3.1 Pre-analysis procedures

Geometries for both concrete and steel parts were created as *3D deformable solids* from revolution around their central vertical axis, with the linear elastic material properties in Table 4. The values follow Svensson [7]; therefore, the analysis is limited to a deterministic approach and does not consider uncertainty in materials' properties. *Tie constraints* were applied between the material interfaces to establish the assumed condition of perfect adherence and boundary conditions constraining translational degrees of freedom were applied in the initial step to the bottom surface of the foundation.

For the models presented, the C3D8R element was chosen: an 8-node linear brick, reduced integration with hourglass control element, compatible with the analyses' scopes according to Hemanth's [14] benchmark analysis and the Abaqus documentation [15].

Table 4. Material properties

| Materials | Young's Modulus (Pa) | Poisson's Ratio | Density (kg/m³) |
|---|---|---|---|
| Concrete | 2.70E+10 | 0.20 | 2400 |
| Steel | 2.00E+11 | 0.29 | 7800 |

## 3.2 Linear-static analysis

All the static loads obtained in section 2.4 (Table 2 and Table 3) were applied to a central reference point (Figure 10), which couples the rigid body motion of the nodes on the top surface of the embedded ring's superior flange, to represent the transmission of forces by the wind turbine tower to the foundation. The foundation's self-weight, *w,* was also considered for the analysis.

A mesh convergence analysis was carried out (Table 5), where the refinement was conducted progressively to compare, for the three points in Figure 10**,** the Y-axis normal stress ($S_{22}$) behavior. The results from the six meshes can be seen in Figure 11**,** where mesh four marks the point where the size of the elements no longer influences the outcome. That is, therefore, the mesh chosen for the analyses.

Table 5. Mesh convergence analysis

| Mesh ID | # Elements | # Nodes | Normal stress ($S_{22}$) (MPa) Point A | Point B | Point C |
|---|---|---|---|---|---|
| 1 | 2856 | 3667 | -0.4976 | -0.3135 | -0.0173 |
| 2 | 7328 | 8692 | -0.4526 | -0.2352 | -0.0162 |
| 3 | 13592 | 15989 | -0.4522 | -0.1833 | -0.0180 |
| 4 | 19852 | 23057 | -0.4746 | -0.1460 | -0.0181 |
| 5 | 61692 | 67257 | -0.4717 | -0.1328 | -0.0181 |
| 6 | 153160 | 162396 | -0.4783 | -0.1301 | -0.0180 |

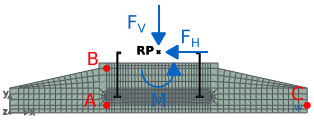


Figure 10. Middle section view with static loads and control points

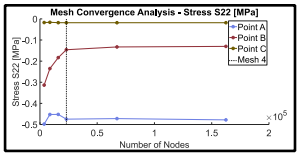


Figure 11. Mesh convergence analysis

## 3.3 Linear-dynamic analysis

In the dynamic scenario, a transient analysis was executed through implicit direct integration, with Rayleigh damping ratios of 5% for concrete and 1% for steel. A convergence analysis for time increments was run for four

specific regions of the structure, defined in terms of sets of two to four elements located in Figure 12, after which the time step of 0.01s was chosen (Figure 13). The transient loads obtained in section 2.5 were applied to the structure for a simulation of 20s in the form of tabular amplitude data, for t=25s to t=45s from Figure 8 and Figure 9. A separate static analysis containing only the gravitational loads from the turbine (Table 2) and the foundation's self-weight was carried out, and the complete results are displayed in the next section.

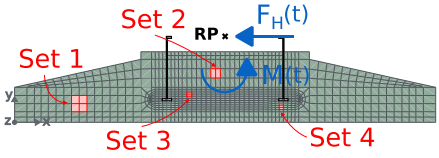


Figure 12. Middle section view with dynamic loads and elements' sets

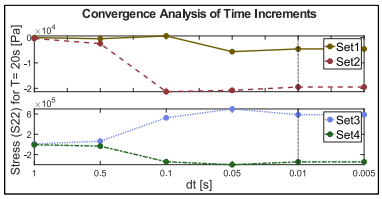


Figure 13. Time increment convergence analysis

### 3.4 Linear-static analysis results

Results from the linear static analysis:

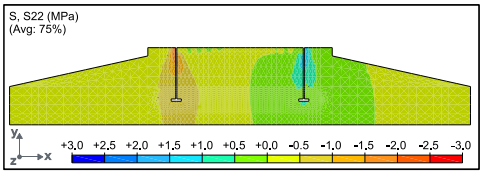


Figure 14. $S_{22}$ stress in the concrete's middle section

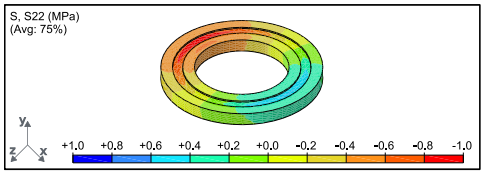


Figure 15. $S_{22}$ stress beneath the bottom flange

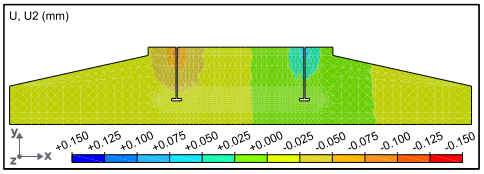


Figure 16. Displacement (*y* axis) in the concrete's middle section

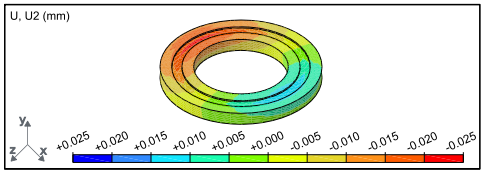


Figure 17. Displacement (*y* axis) beneath the bottom flange

### 3.5 Linear-dynamic analysis results

Results from the linear-dynamic analysis, for t=26s:

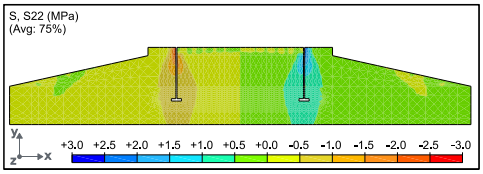


Figure 18. $S_{22}$ stress in the concrete's middle section

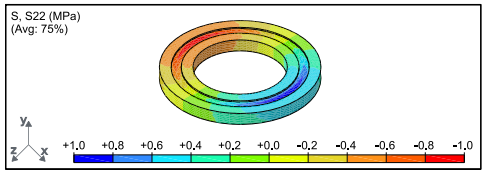


Figure 19. $S_{22}$ stress beneath the bottom flange

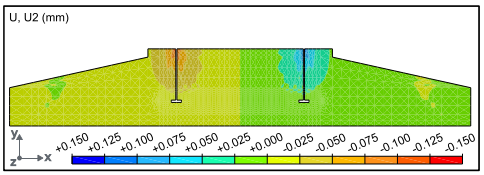


Figure 20. Displacement (*y* axis) in the concrete's middle section

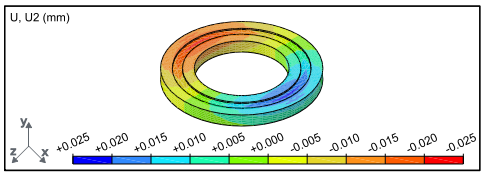


Figure 21. Displacement (*y* axis) beneath the bottom flange

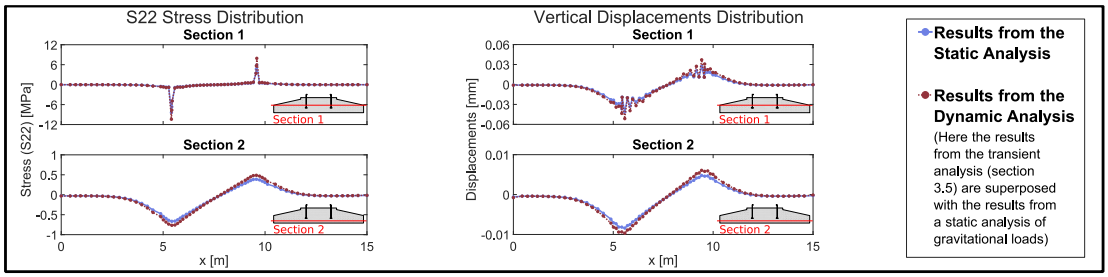


Figure 22. Summary of analyses' results

# 4 Conclusions

This work presented a robust development of a numerical model for the structural analysis of a wind turbine embedded ring foundation, allowing for comparison between two linear analyses: static and dynamic. Figure 22 clearly shows the difference detected between these results for the regions situated closer to the steel ring, with the outputs from the dynamic analysis exceeding the static ones in the pair of sections analyzed for both stress and displacement. It is essential to recall that the dynamic model results did not take into account the wind loads acting over the tower, only on the rotor. However, that component was responsible for only approximately 2% and 3% of the total overturning moment and horizontal force, respectively, from the wind loads used in the static analysis. Furthermore, both analyses resulted in stress concentrations in the concrete surrounding the ring's bottom flange as expected (Figure 15 and Figure 19). Therefore, although still an initial study uncompromised with structural design, this linear model proves a leading tool for investigating deterioration-related issues towards its prevention in future embedded ring foundations and the design of permanent repair solutions for existing structures. Following advancement could be achieved with the inclusion of nonlinearity consideration and analyses of reinforcement and fatigue behaviors.

**Acknowledgements.** This study was financed in part by the Coordenação de Aperfeiçoamento de Pessoal de Nível Superior - Brasil (CAPES) - Finance Code 001.

**Authorship statement.** The authors hereby confirm that they are the sole liable persons responsible for the authorship of this work, and that all material that has been herein included as part of the present paper is either the property (and authorship) of the authors, or has the permission of the owners to be included here.

# References

[1] M. He, X. Bai, R. Ma, D. Huang, Structural monitoring of an onshore wind turbine foundation using strain sensors, Struct Infrastruct E. 15 (2019) 1–20. https://doi.org/10.1080/15732479.2018.1546325.
[2] M. Hassanzadeh, Cracks in onshore wind power foundations, Stockholm, 2012.
[3] M. Currie, C. Tachtatzis, M. Saafi, F. Quail, Structural Health Monitoring System for Wind Turbine Foundations, in: Vienna, Austria, 2013. https://doi.org/10.13140/2.1.1418.6881.
[4] M. Currie, M. Saafi, C. Tachtatzis, F. Quail, Structural integrity monitoring of onshore wind turbine concrete foundations, Renew Energ. 83 (2015) 1131–1138. https://doi.org/10.1016/j.renene.2015.05.006.
[5] D.L. Logan, A First Course in the Finite Element Method, 6th ed., Cengage Learning, Boston, USA, 2016.
[6] S.S. Rao, The finite element method in engineering, Elsevier, 2018.
[7] H. Svensson, Design of Foundation of Wind Turbines, 2010.
[8] Product brochure V90-1.8/2.0 MW, (2009). https://www.collgarwindfarm.com.au/wp-content/uploads/2015/01/Vestas_Product-brochure-V90-1.8-2.0MW-06-09-EN.pdf (accessed June 26, 2020).
[9] General Specification V90–1.8/2.0 MW 50 Hz VCS, (2010).
[10] H. Kawai, K. Michishita, A. Deguchi, Design Wind Loads On A Wind Turbine For Strong Wind, in: 2008.
[11] M. Perry, J. McAlorum, G. Fusiek, P. Niewczas, I. McKeeman, T. Rubert, Crack Monitoring of Operational Wind Turbine Foundations, Sensors. 17 (2017) 1925. https://doi.org/10.3390/s17081925.
[12] D.C.F. BARROS, ANÁLISE DINÂMICA DE AEROGERADORES OFFSHORE COM FUNDAÇÃO TIPO MONOPILAR, 2020.
[13] R.A. Kjørlaug, Seismic Response of Wind Turbines - Dynamic Analysis of a Wind Turbine in Horizontal and Vertical Direction - Subject to Earthquake, Wind & SSI, 2013.
[14] R.H. Hemanth, P. Ruchin, G. Gourav, G.V.V.R. Kumar, K.S. Venkatesha, H. Sklyut, M. Kulak, M. Heinimann, Performance Evaluation of Finite Elements for Analysis of Advanced Hybrid Laminates, (2010).